JOURNAL OF CATALYSIS 151, 168–177 (1995)

Rh-Loaded CeO_2–ZrO_2 Solid Solutions as Highly Efficient Oxygen Exchangers: Dependence of the Reduction Behavior and the Oxygen Storage Capacity on the Structural Properties

P. Fornasiero,* R. Di Monte,† G. Ranga Rao,‡ J. Kašpar,*[,1] S. Meriani,† A. Trovarelli,§ and M. Graziani*

* *Dipartimento di Scienze Chimiche, Università di Trieste, Via Giorgieri 1, 34127 Trieste, Italy;* † *Dipartimento di Ingegneria dei Materiali e Chimica Applicata, Università di Trieste, Via Valerio 2, 34127 Trieste, Italy;* ‡ *International Centre for Science and High Technology, APH Grignano, 34100 Trieste, Italy; and* § *Dipartimento di Scienze e Tecnologie Chimiche, Via Cotonificio 108, 33100 Udine, Italy*

Received January 31, 1994; revised May 25, 1994

Temperature-programmed reduction in a H_2/Ar mixture of Rh-loaded CeO_2–ZrO_2 solid solutions with a ZrO_2 content varying between 10 and 90% mol and of monoclinic, tetragonal, and cubic structures is reported. It is shown that incorporation of ZrO_2 into a solid solution with CeO_2 strongly promotes bulk reduction of the Rh-loaded solid solutions in comparison to a Rh/CeO_2 sample. The promotion of the bulk reduction results in high oxygen storage capacity (OSC) as measured by oxygen uptake. A structural dependence of both reduction and oxidation processes is observed which is attributed to a higher oxygen mobility in the cubic structure compared to the tetragonal and monoclinic ones. © 1995 Academic Press, Inc.

INTRODUCTION

Cerium oxide is widely employed as a promoter for noble-metal/alumina automotive exhaust catalysts. The suggested promoting roles of this component are the following: (i) stabilization of the metal dispersion and of the alumina support, (ii) promotion of the water–gas shift reaction, and (iii) enhanced oxygen storage and release by shifting between CeO_2 under oxidizing conditions and Ce_2O_3 under reducing conditions, respectively (1). Among these functions, high oxygen storage capacity (OSC) of a three-way catalyst (TWC) is an important property in vehicle application since it allows one to enlarge the operating air/fuel (A/F) window, thereby making the catalyst less sensitive to small temporary variations of A/F. OSC provided by Ce^{3+} also plays a crucial role in enhancing the activity in reducing conditions, i.e., fuel-rich conditions, since more oxygen is available for the oxidation processes (2). Furthermore, the oxygen vacancies associated with reduced ceria in the proximity of noble-metal particles have been suggested as promoting sites for NO and CO conversion (2, 3).

Recently, we reported (4) that NO is effectively decomposed at the Ce^{3+} sites in the Rh- and Pt-loaded Ce-containing materials, suggesting a direct participation of the reduced support in the NO conversion. It was also observed that upon incorporation of ZrO_2 into a solid solution with CeO_2, the reducibility of the Ce^{4+} is strongly enhanced compared to pure CeO_2 both in the unsupported (5) and metal-loaded samples (4). As a matter of fact, in the presence of H_2, a Rh/$Ce_{0.6}Zr_{0.4}O_2$ sample was reduced in the bulk at temperatures as low as 673 K (4). This suggests that such a system, when operating in a reducing environment such as the fuel-rich conditions, could effectively decompose NO at the Ce^{3+} sites which results in an enhanced NO removal efficiency of the catalyst in the low-temperature regimes. NO decomposition occurred indeed at temperatures as low as 473 K (4). Enhanced catalytic activities at low temperatures are highly desirable. In order to minimize vehicle emissions during the cold start, the majority of vehicle applications utilize close-coupled catalyst locations. This results in extreme catalyst temperatures which may exceed 1100 K at high driving speeds, causing deactivation due to sintering.

Noteworthy is that a quantitative estimation of the amount of oxygen released and regained in the reduction–oxidation cycle showed that the bulk of the support material was involved (4). According to the cerium content, the ceria–zirconia solid solutions exist in three different structures, namely monoclinic, tetragonal, and cubic (6). Pal'guev *et al.* (7) showed that the dimensions of the unit cell decrease linearly on decreasing the cerium content from 100 to 50% mol. At the same time, from density measurements, they observed a decrease in the number of atoms present in the cell, which denotes the

[1] To whom correspondence should be addressed.

0021-9517/95 $6.00

presence of structural defects. Therefore, keeping in mind that the bulk of the material is involved in the reduction–oxidation cycles, structural dependence of the oxygen storage capacity may be expected and this is addressed in the present paper. It is shown that, despite the very low surface area of the investigated samples, high OSC is observed after a reducing pretreatment at a temperature as low as 700 K. Moreover, the OSC is strongly favored by the presence of the cubic structure as compared to the tetragonal one. In forthcoming papers (8) we will report the effects of prereduction of the present metal-loaded CeO_2–ZrO_2 solid solutions both on the activity in the reduction of NO by CO and on the decomposition of NO in comparison with a Rh/CeO_2 sample. Moreover, investigation of high surface area metal-loaded CeO_2–ZrO_2 solid solutions discloses that the presence of reduced support sites strongly enhances the catalytic activity in the reduction of NO by CO showing the crucial role of the Ce^{3+} sites in the dissociation of NO.

TABLE 1

Composition and Properties of the as-Synthesized CeO_2–ZrO_2 Solid Solutions

CeO_2 content (% mol)	Cell volume (Å^3)	Pycnometric density (g ml^{-1})	n_{MO_2}[a]	Phase composition[b] (%)
10	144.02	5.70		TZ°(5), Monoclinic (95)
20	138.69	5.86	3.74	TZ°
30	140.10	5.98	3.76	TZ°(78), TZ′(11), Cubic(10)
40	145.80	6.00	3.73	TZ°(36), TZ′(53), Cubic(10)
50	147.06	6.22	3.73	TZ′
50	148.17	6.11	3.69	Cubic
60	149.46	6.41	3.78	Cubic
70	153.97	6.66	3.92	Cubic
80	154.74	6.88	3.95	Cubic
90	156.24	7.07	3.98	Cubic
100	157.60	7.23	3.99	Cubic

[a] Calculated from Eq. [1].
[b] Estimated from XRD results.

EXPERIMENTAL

CeO_2–ZrO_2 solid solutions with CeO_2 molar content ranging from 10 to 90% were prepared by firing in air a mixture of the oxides (CeO_2, Medolla; ZrO_2, Harshaw 102) of appropriate composition at 1873 K for 1 h and then cooling to room temperature at a rate of 10 K min^{-1}. Powder X-ray diffraction patterns were collected on a Siemens Kristalloflex Model F Instrument, (Ni-filtered Cu$K\alpha$). Sample densities were measured on a Quantachrome Corporation Multipycnometer. Single-point BET area measurements were carried out on a Micromeritics surface area analyzer by N_2 adsorption at 77 K. The measurements suggested an upper limit of surface area of about 1–2 m^2 g^{-1} for all the samples. A summary of the properties of the employed samples is reported in Table 1.

Supports were impregnated with $RhCl_3 \cdot 3H_2O$ or $Na_2PtCl_6 \cdot nH_2O$ to incipient wetness; afterward the catalysts were dried at 393 K overnight. This procedure was repeated 5–7 times until the nominal metal loading of 0.5 wt% was attained. The samples were then calcined at 723 K for 5 h. Temperature-programmed reduction (TPR) experiments were carried out either in a conventional system or in a TG-DTA apparatus. The former was equipped with a thermal conductivity detector and the reduction was carried out in flow of H_2 (5%) in Ar (25 ml min^{-1}) using a heating rate of 10 K min^{-1}. Typically, the reduction was carried out up to 1273 K and then the sample (0.04–0.07 g) was held at this temperature for 30 min. The amount of H_2 uptake in the TPR was estimated from integrated peak areas by comparison with those obtained by using CuO as a standard. The reproducibility of the method was periodically checked and a standard deviation for the overall H_2 uptake of ± 1.0 ml g^{-1} was measured. Standard deviations observed for the peak temperatures of the three peaks reported in Fig. 1 (see below) were respectively ± 5 K, ± 25 K, and ± 35 K. It should be noted that these standard deviations were obtained over a series of samples prepared separately by replicating both synthesis of the support and metal precursor deposition. OSC was measured by pulse technique in the same equipment used for the TPR experiments. The samples were reduced in H_2/Ar mixture (10 K min^{-1} to 700 K and then held for 2 h). H_2 was then desorbed in Ar flow (20 ml min^{-1}) at 700 K for 2 h. The oxygen uptake was measured by injecting pulses of O_2 (0.092 ml) into the flow of Ar passing over the catalyst (0.04–0.05 g) until the breakthrough point was attained.

RESULTS

Characterization of the Supports

As stated above, there are three possible structures (monoclinic, tetragonal, and cubic) for the binary system CeO_2–ZrO_2. Below 1300 K the monoclinic and cubic phases appear to be thermodynamically stable; however, when the ceramic method is employed for the synthesis of the solid solution, the metastable tetragonal phase is easily formed in a wide compositional interval and it is fairly stable at ordinary temperatures (9). A non-quenching cooling rate produces two phases of tetragonal symmetry referred to as TZ° and TZ′ (9). These phases exist pure in the compositional range 5–20% CeO_2 and 40–60% CeO_2, respectively, while at a CeO_2 content of

20–40%, a mixture of TZ° and TZ′ is obtained. The former phase is characterized by a larger orthogonality ($c/a \approx 1.018$) compared to the TZ′ phase ($c/a. \approx 1.010$) (9b). Both tetragonal TZ° and TZ′ phases were detected in the present samples. The estimated phase composition, XRD characterization of the samples and density measurements are reported in Table 1.

Phase composition of all the samples except $Ce_{0.1}Zr_{0.9}O_2$ appears to be consistent with previous reports (9, 10); i.e., at low CeO_2 content TZ° formation is favored while in the region 30–50% of CeO_2 formation of the TZ′ phase occurs but it is strongly dependent on the cooling rate. Low cooling rates favor TZ′ formation while by quenching the mixture to room temperature, formation of a cubic phase is favored (10). Detection of a monoclinic phase for the $Ce_{0.1}Zr_{0.9}O_2$ sample can be attributed to a lower cooling rate employed here compared to the previous study (9). On increasing the CeO_2 content, the unit cell volume increases because of the greater ionic radius of the 8-coordinated Ce^{4+} ion (0.97 Å) compared to Zr^{4+} (0.84 Å) (11). Table 1 also reports the number of formula units (n_{MO_2}, M = Zr, Ce) in the elementary cell calculated from the formula (12)

$$n_{MO_2} = \frac{\rho V}{1.6602\ \mathrm{MW}} \qquad [1]$$

where ρ = pycnometric density (g ml^{-1}); V = unit cell volume (Å^3), and MW = molecular weight.

The values of the number of MO_2 units are significantly lower than four which suggests that incorporation of ZrO_2 into CeO_2 favors formation of structural defects in the solid solutions. The defective structure could be associated with the presence of oxygen vacancies due to an incomplete Ce^{3+} reoxidation in the course of the cooling process. Also the presence of small amounts of a cubic phase observed in the samples containing 30 and 40% of CeO_2 may suggest a relatively rapid cooling rate which prevents a full Ce^{3+} reoxidation. However, further observations point to a different nature of the defective structure. The as-prepared solid solutions showed a yellow to light-gray color suggesting that most of Ce^{3+} was reoxidized in the cooling process. Annealing of the samples in air at 523 K did not significantly increase their densities suggesting that no further reoxidation occurred. Moreover, the $Rh/Ce_{0.6}Zr_{0.4}O_2$ sample showed no measurable paramagnetism attributable to the presence of Ce^{3+} species (8). All these observations suggest that the defective structure of the present samples should not only be associated with oxygen vacancies, but both oxygen and metal vacancies are formed.

A purely cubic $CeO_{0.5}Zr_{0.5}O_2$ sample was obtained by a rapid quenching from 1973 K to room temperature according to Ref. (10).

Temperature-Programmed Reduction

Figure 1 shows the hydrogen uptakes as a function of temperature obtained for the calcined Rh-loaded ceria–zirconia samples. Three peaks with maxima at 350–390 K, 600–950 K, and 1050–1250 K, respectively, are observed for most of the samples. The relative intensities of the peaks above 500 K strongly depend on CeO_2 content: there is only a single peak in the high-temperature region for the Rh/CeO_2 sample while, in the case of the solid solutions, the intensity of this peak is negligible for CeO_2 contents less than 40%. For the $Rh/Ce_{0.1}Zr_{0.9}O_2$ (Fig. 1, trace 2), the peak at intermediate temperature is centered at about 925 K. Occasionally, an additional feature at 420 K is found; compare, for example, the $Rh/CeO_{0.8}Zr_{0.2}O_2$ sample.

For the reader's convenience, the attribution of the TPR peaks will be discussed in this section. The peaks below 500 K are attributed to reduction of the rhodium oxide precursor. The presence of two peaks for the Rh_2O_3 reduction may be attributed to a nonuniform size distribution of the Rh_2O_3 particles. The peak at the lower temperature should be associated with well-dispersed metal oxide while the other peak is associated with pres-

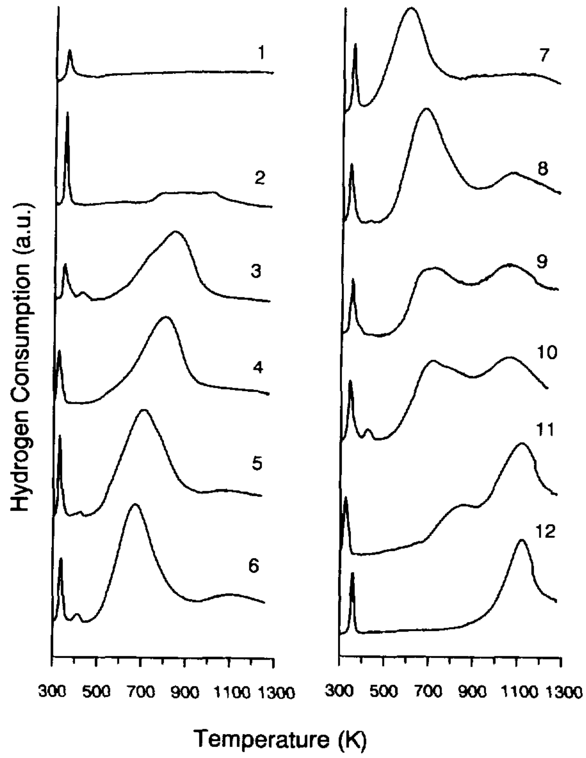

FIG. 1. Normalized TPR profiles of calcined Rh-loaded CeO_2–ZrO_2 and CeO_2: Rh/ZrO_2 (1), $Rh/Ce_{0.1}Zr_{0.9}O_2$ (2), $Rh/Ce_{0.2}Zr_{0.8}O_2$ (3), $Rh/Ce_{0.3}Zr_{0.7}O_2$ (4), $Rh/Ce_{0.4}Zr_{0.6}O_2$ (5), tetragonal (TZ′) $Rh/Ce_{0.5}Zr_{0.5}O_2$ (6), cubic $Rh/Ce_{0.5}Zr_{0.5}O_2$ (7), $Rh/Ce_{0.6}Zr_{0.4}O_2$ (8), $Rh/Ce_{0.7}Zr_{0.3}O_2$ (9), $Rh/Ce_{0.8}Zr_{0.2}O_2$ (10), $Rh/Ce_{0.9}Zr_{0.1}O_2$ (11), and Rh/CeO_2 (12).

ence of bulk-like crystalline Rh_2O_3 on the surface (13). The presence of large Rh_2O_3 crystals is reasonable in view of the low surface area of the supports. Consistently with the above attribution, unsupported ceria–zirconia samples show no hydrogen consumption below 500 K (4, 5). Alternatively, as suggested by an anonymous referee, the possibility of some inhomogeneity of the surface of the solid solution cannot be excluded. Similarly, albeit that the shifts observed in Fig. 1 for the peaks attributed to Rh_2O_3 reduction are significant, they are best attributed to the difficulty of obtaining a homogeneous distribution of the metal oxide precursor in the different samples due to their very low surface areas.

The peaks above 500 K are therefore associated with the reduction of the support. TPR of pure CeO_2 generally shows two peaks at approximately 770 and 1100 K, the former being associated with surface reduction (1d) even though there is now evidence that nonstoichiometric CeO_x ($x < 2$) phases can also be formed (14, 15). However, when a low surface area sample is employed, this peak is negligible and it appears as a shoulder of the peak due to bulk reduction at 1100 K (1d, 16). In the presence of the metal, the peak at 770 K is shifted to lower temperatures and split into several peaks (1d, 16). In the course of the TPR, metal particles cause spill-over of hydrogen onto the support inducing a concurrent reduction of both the metal oxide precursor and the surface of CeO_2 (2, 17, 18).

A striking modification of the reduction behavior of the Rh-loaded samples is observed for CeO_2–ZrO_2 solid solutions with respect to pure CeO_2, as shown in Fig. 1. There is a very strong promotion of the reducibility of the support as shown by the appearance of a new peak at 600–950 K. (Henceforth, the feature at 600–950 K will be indicated as the LT, viz. low temperature, peak and the feature above 950 K as the HT, viz. high temperature, peak.) Accordingly, the LT and HT features have to be associated with the reduction of the bulk solid solutions.

It should be noted that the temperature of the maximum of the LT peak strongly depends on the nature of the sample. It decreases on decreasing the cerium molar content from 90 to 60%, while further decrease from 50 to 10% broadens and shifts the LT peak to higher temperatures. A summary of the results of the TPR experiments carried out on all the Rh-loaded samples is reported in Table 2.

Some interesting features immediately appear from a perusal of Table 2: formation of a solid solution between ceria and zirconia, which strongly promotes the reduction of the support as a new reduction feature with a maximum below 950 K, is always observed. The splitting of the support reduction process into two peaks heavily depends on CeO_2 content. The ratio of the LT/HT peak areas increases on decreasing the percentage of CeO_2. The degree of support reduction is therefore reported both after the LT and HT peaks, the latter value corre-

TABLE 2

TPR of Rh- and Pt-Loaded CeO_2–ZrO_2 Solid Solutions and CeO_2[a]

CeO_2 content (% mol)	Peak temperatures for support reduction (K) LT peak	HT peak	Degree of reduction[b] After LT peak $CeZrO_x$	CeO_yZrO_2	After HT peak $CeZrO_x$	CeO_yZrO_2	Ratio of peak areas LT/HT
10	925		1.95	1.51	1.95	1.51	—
20	850		1.91	1.58	1.91	1.52	—
30	810		1.87	1.57	1.87	1.57	—
40	700	1100	1.88	1.57	1.83	1.57	—
50[c]	670	1110	1.87	1.74	1.80	1.59	2.0
50[d]	600	1080	1.87	1.75	1.80	1.60	1.9
60	670	1085	1.87	1.78	1.77	1.61	1.4
60[e]	680	1100	1.86	1.76	1.76	1.60	1.4
70	700	1055	1.92	1.88	1.77	1.68	0.6
80	715	1055	1.91	1.88	1.75	1.69	0.6
90	840	1105	1.96	1.95	1.79	1.77	0.3
100		1110			1.80	1.80	0.0

[a] Sample characteristics as reported in Table 1.

[b] x and y: degree of reduction as defined in the text; "after HT" signifies overall degree of reduction. Replicate experiments carried out over several samples showed a standard deviation $y < 0.02$.

[c] Tetragonal sample (TZ′).

[d] Cubic sample.

[e] Pt-loaded sample.

sponding to the overall TPR. Support reduction can be associated with the formation of anionic oxygen vacancies in the solid solution due to the reducible Ce^{4+} cations (19). Consistently, the Rh/ZrO_2 catalyst (Fig. 1, trace 1) shows no reduction peak in the range of temperatures 500–1200 K. Table 2, therefore, reports the degree of reduction both as x in $Ce_mZr_{(1-m)}O_x$ (m = Ce molar fraction), where $2 - x$ represents the total amount of oxygen vacancies formed by the reduction of the solid solution, and as y in $mCeO_y(1 - m)ZrO_2$, i.e., by associating the oxygen vacancies with Ce^{3+} sites. Thus the value of x gives an estimation of the total degree of reduction while in the latter formula y is a measure of the extent of Ce^{4+} reduction in the TPR. The value of $y = 1.5$ corresponds to the reduction to Ce^{3+} of all the Ce^{4+} initially present. Obviously in the case of pure ceria x is equal to y. As is shown below, reoxidation of the reduced support occurs easily above 473 K and therefore the value of x also reflects the total OSC of the support.

Recently, Zotin *et al.* (20) warned about the reliability of the measurements of degree of cerium reduction from the TPR experiments, since adsorbed species may invalidate quantitative estimation. Our results show that such considerations are not valid for samples of a low surface area like those used here. Consistently, in the reoxidation of the catalysts, we found O_2 adsorption to be closely related to the initial degree of reduction as estimated from TPR (compare Table 3).

As reported in Table 2, the final degree of reduction in the Rh/CeO_2 sample is $x = y = 1.80$. In a reducing environment or at high temperatures, CeO_2 loses oxygen to give suboxides of the type CeO_x ($x < 2$). Above 1273 K, x continuously changes in the range $1.72 \le x \le 2.00$ while at lower temperatures ceria forms a series of discrete stoichiometries Ce_nO_{2n-2} (6, 19 and references therein). The value of $x = 1.80$ suggests that formation of some species with $n = 10$ might occur. This is consistent with previous studies which showed that prolonged reduction of CeO_2 at 773 and 900 K leads, respectively, to $CeO_{1.90}$ (21) and $CeO_{1.82}$ (14), which can be associated with the formation of discrete suboxide phases (6, 19). It is worth noting that in a reducing environment, the CeO_2–ZrO_2 solid solutions should be more properly considered as a ternary ZrO_2–CeO_2–Ce_2O_3 system. The phase diagram does not show distinct nonstoichiometric phases as in the case of CeO_{2-x} except for a cubic $Ce_2Zr_2O_7$ compound with the pyrochlore structure which is present in the system $CeO_{1.5}$–ZrO_2 (6). Therefore no straightforward attri-

TABLE 3

Hydrogen Consumption and Oxygen Uptake over Rh/CeO_2 and Rh/CeO_2–ZrO_2 Solid Solutions

Run	CeO_2 content (% mol)	H_2 consumption[a] (ml g^{-1})	O_2 uptake: Temperature (K)	Amount (ml g^{-1})	Amount mol O_2/mol Ce (×100)	Activation energy and standard deviation (kcal mol^{-1})
1	100[b]	26.2	700	4.5	3.2	
2	100[c]	8.6	700	3.9	2.7	
3	100[d]	1.4	700	0.16	0.11	3.40 ± 0.15
			600	0.12	0.09	
			550	0.10	0.07	
4	60	16.2	700	8.0 (8.0)[e]	8.3 (8.3)[e]	2.05 ± 0.12
			600	7.5	7.8	
			500	6.2	6.4	
5	50[f]	17.3	700	8.8	10.6	1.84 ± 0.15
			600	8.4	10.2	
			550	7.8	9.4	
6	50[g]	18.3	700	9.4	11.3	1.73 ± 0.08
			600	9.0	10.9	
			550	8.5	10.3	

[a] Hydrogen consumed in the TPR preceeding the OSC measurement (see Experimental).
[b] Surface area 130 m^2 g^{-1}.
[c] Surface area 30 m^2 g^{-1}.
[d] Surface area 1.5 m^2 g^{-1}.
[e] Catalyst recycled twice.
[f] Tetragonal sample (TZ′).
[g] Cubic sample.

bution of the final or intermediate degree of reduction can be made.

As discussed above, we relate the reduction to formation of Ce^{3+} which is also supported by measurements of magnetic susceptibility over reduced Rh/$Ce_{0.6}Zr_{0.4}O_2$ (4, 8) which showed a close correspondence between the value of y as measured from TPR and that estimated according to Ref. (14) from this technique.

The data reported in Table 2 clearly suggest an optimal range of composition (40–60% of CeO_2) for obtaining a high degree of reduction at low (600–700 K) temperatures. For lower CeO_2 contents, an almost complete reduction of Ce^{4+} to Ce^{3+} is observed (y = 1.51 and 1.52 for $Ce_{0.1}Zr_{0.9}O_2$ and $Ce_{0.2}Zr_{0.8}O_2$ samples, respectively); however, the overall degree of reduction is much lower, indicating that for these samples the amount of CeO_2 present is the factor limiting the degree of reduction. Notably, the LT peak also shifts toward higher temperatures on decreasing the CeO_2 content. Similarly for $CeO_2 > 60\%$, the LT peak shifts toward higher temperatures. The ratio of LT/HT peak areas monotonically increases on decreasing the CeO_2 content indicating that the LT feature is more pronounced for low CeO_2 content.

Significantly, while the degree of reduction of the $Ce_{0.5}Zr_{0.5}O_2$ samples appears almost unaffected by the structure of the sample, the maximum of the LT peak for the cubic sample is 70 K lower than for the tetragonal one.

Summarizing, it clearly appears from the TPR results that there is an optimum range of composition (CeO_2 = 40–60%) where highest degree of support reduction (x) and lowest reduction temperatures are observed and that in the cubic structure the reduction process is kinetically favored compared to the tetragonal one.

Oxygen Storage Capacity of Reduced Samples

On the basis of the TPR results we carried out selected OSC measurements by the pulse technique described under Experimental (Table 3). For the sake of comparison, the amount of H_2 consumed in the reduction preceding the OSC measurement is included.

As pointed out by Cho (22), in the OSC measurement by the pulse method, the oxygen uptake is controlled by the mobility of oxygen at a given temperature rather than by the ultimate oxygen storage capacity of the support which in fact is independent of the temperature. Consistently, for the CeO_2 samples, the hydrogen uptake in the TPR is always more than the oxygen uptake corresponding to full reoxidation of the carrier. Since CeO_x ($x < 2$) reoxidation is reported to be a fast and reversible reaction (14), the contribution of adsorbed species to the total H_2 uptake in the case of high surface areas cannot be disregarded (20). CeO_2 has a great affinity for hydrogen atoms and hydrogen fixation is to a large extent reversible (18), even after a reduction at 623 K (23). Such contributions should be insignificant for the low surface area samples. The Rh/CeO_2 samples show a significant increase of oxygen uptake on increasing the surface area. This is consistent with the attribution of the oxygen storage mainly to surface redox processes since surface reduction is strongly favored on high surface area CeO_2 (1d, 16).

The high values of the OSC observed for the three Rh-loaded CeO_2–ZrO_2 samples here investigated must be associated with a bulk redox process. It is worth noting that, in the range of temperatures investigated (500–700 K), all the solid solutions (Table 3, runs 4–6) take up significantly more oxygen than Rh/CeO_2 (Table 3, run 1) despite a difference of two orders of magnitude in the surface areas. The increased efficiency of the $Ce^{3+} \leftrightarrow Ce^{4+}$ redox cycle is more evident when the OSC values are compared in terms of moles O_2 uptake/moles Ce (Table 3). Notably, recycling of the catalyst does not influence the OSC (run 4, Table 3). Conversely, the TPR profile for the support reduction of the reduced and reoxidized catalyst is unaffected by the redox cycles. Finally, the activation energy for oxygen uptake significantly decreases upon incorporating CeO_2 into ZrO_2. Consistently with the TPR measurements, the most favorable activation energy is observed for the cubic $Ce_{0.5}Zr_{0.5}O_2$ sample.

DISCUSSION

The most important observation of the present results is that incorporation of even relatively low amounts of ZrO_2 into the CeO_2 framework strongly promotes in the metal-loaded samples the reduction of the support in the bulk. This results in a remarkable enhancement of oxygen storage and release capacities as shown in temperature-programmed reduction and oxygen uptake measurements. This is attributed to a bulk reduction which is occurring in the metal-loaded solid solutions at fairly low temperatures compared to CeO_2. At variance with this, the OSC of Rh/CeO_2 is strongly dependent on the surface area and is rather limited in the sample calcined at 1873 K (Table 3). Thermal aging in oxidizing conditions leads to both to a growth of CeO_2 crystallites (24) and a net decrease of three-way catalyst performances which were associated with a decline of CeO_2 surface area (2). The present findings, that OSC of the metal-loaded CeO_2–ZrO_2 solid solutions does not decline even for very low surface areas, may represent an interesting breakthrough point for the TWC catalysts. Consistently, we showed in a preliminary report (4) that the bulk oxygen vacancies which are created by the reduction of the Rh/CeO_2–ZrO_2 catalysts directly participate in the conversion of NO.

It is important to recall that our previous investigation (4) showed the crucial role of the metal in promoting the low-temperature reduction of the bulk of the solid solution. In its absence, no LT feature was observed. This was attributed to the ability of the supported metal (Rh or Pt) to activate H_2 and then to spill it over onto the support. In the absence of the metal, due to the low surface area and hence availability of surface OH groups, H_2 activation is difficult and may become rate-determining. Noteworthy is that the reduction process of the support does not depend on the nature of the supported metal. The appearance of the TPR curves reported in Ref. (4) showed a similar profile for support reduction in both the Rh- and Pt-loaded samples. The close agreement between the H_2 consumption of the Rh- and Pt-loaded $Ce_{0.6}Zr_{0.4}O_2$ samples reported in Table 2 is consistent with such a picture. Therefore, the changes in both the peak temperatures and the relative intensities of the peaks above 500 K due to support reduction (Fig. 1) are strictly related to the nature of the solid solution.

Reduction of CeO_2 is suggested to proceed initially via a surface reduction and then on increasing the temperature bulk reduction occurs through a diffusion-limited process (14, 21). Diffusion through grain boundaries could also limit the oxygen mobility (25a); however, it was shown that rhodium ions can be incorporated into the CeO_2 lattice upon calcination (26) and the strong interaction between Rh and CeO_2 then promotes oxygen migration from CeO_2 to Rh (27). Consequently, while oxygen migration in the pure support might be limited by the grain boundary diffusion, it is unlikely that in the presence of the metal it remains the rate limiting factor. Moreover, Ando *et al.* (28) observed that the oxygen self-diffusion coefficient was enhanced by a rapid grain growth in the CeO_2–ZrO_2 solid solutions, which was interpreted by creation of a fast diffusion layer at the grain boundary. On the basis of these considerations it appears reasonable that the bulk diffusion is the slowest step of the reduction process while both grain boundary and surface diffusion are faster. The oxygen diffusion in the fluorite structure is much faster compared to the metal diffusion (25b), and therefore the kinetics of the bulk reduction depend upon restrictions to the oxygen diffusion. Thus it is important to analyze carefully the structural parameters of the present samples to understand the reasons underlying the observed phenomenon.

The XRD measurements show that in the present solid solutions, the cell parameters decrease linearly with decreasing CeO_2 content according to the Végard law (9). As shown in Fig. 2, the unit cell volume decreases linearly with decreasing CeO_2 content in the range of composition 100–40%, i.e., cubic and TZ′ samples, while for lower CeO_2 contents (monoclinic and TZ° samples), significant deviations occur. Notably, also the cubic

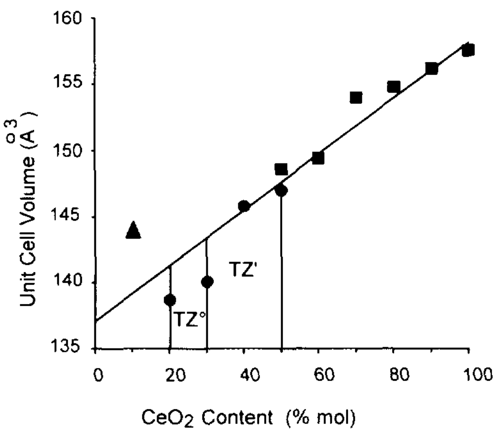

FIG. 2. Unit cell volume vs CeO_2 content of the as prepared monoclinic (▲), tetragonal (●), and cubic (■) CeO_2–ZrO_2 and CeO_2 supports.

$Ce_{0.5}Zr_{0.5}O_2$ sample prepared by the quenching method (see above) properly fits the line of the other cubic samples. The very small negative deviation of the TZ′ sample from the line of the cubic samples is due to the fact that the TZ′ structure is a slight distortion along the c axis of the CeO_2 cubic cell (fcc, space group Fm3m (29)). Consequently, the unit cell volume is closely related to the cubic CeO_2. At variance with this, the TZ° structure is a distortion of the tetragonal ZrO_2 (space group $P4_2/nmc$ (29)) and therefore the unit cell volume is related to a pure tetragonal ZrO_2. Consistently, both TZ° and tetragonal ZrO_2 have the same degree of tetragonality (c/a = 1.018). The relatively high value of the cell volume observed for the $Ce_{0.1}Zr_{0.9}O_2$ is due to the presence of the monoclinic phase. For comparison, pure monoclinic ZrO_2 has a cell volume of 140.52 Å^3.

The oxygen diffusion in the defective fluorite structure of CeO_2 can be described by a vacancy mechanism (30). Therefore, a smaller cell volume should require less energy for the activated hopping of oxygen ions within the lattice and favor the reduction. This consideration would suggest that increasing amount of ZrO_2 should always favor the reduction process. Peak temperatures in the TPR experiments depend on the kinetics of the reduction and therefore on the oxygen mobility. A perusal of the data reported in Table 2 shows that the temperatures of both the LT and HT peaks decrease upon increasing up to 50% the ZrO_2 content in the solid solution as long as the cubic structure is preserved. On the other hand, in the presence of the tetragonal structure, the temperatures of the LT and HT peak increase upon increasing the ZrO_2 content. This result is conflicting with the above suggestion that increasing ZrO_2 content should always favor oxygen mobility. A possible explanation for this behavior can be derived by considering the anisotropy of the diffusion in a tetragonal structure. Orientation dependence of mass transport was observed for a boron–silicon system (31) and for a polycrystalline β-alumina (32a). In a polycrystalline system, because of the different orientations of the grain boundaries, the anisotropy of the diffusion will limit the overall rate of diffusion. Accordingly, the tetragonality (c/a) of the tetragonal solution increases from 1.010 to 1.018 on increasing the ZrO_2 content from 60 to 80%, which should hinder the oxygen mobility.

The oxygen mobility may depend on the effective cation radius (31b, 33). The oxygen anions are in a tetrahedral coordination in the fluorite structure, and their migration to the nearby tetrahedral position occurs through channels formed by neighboring cations. The radius (R_f) of these channels is given by

$$R_f = \frac{a}{\sqrt{6}} - r_c,$$

where a is the lattice parameter and r_c is the average cation radius.

Similarly, the following relation can be derived for the tetragonal structure, where a and c are lattice parameters,

$$R_f = \frac{a^2 + c^2}{2\sqrt{2(a^2 + 2c^2)}} - r_c.$$

Dependence of the channel radius upon CeO_2 content is reported in Fig. 3. For the tetragonal structure, R_f is almost invariant with CeO_2 content. At variance with this, in the cubic structure for lower CeO_2 contents, higher R_f are observed. With the exception of the point at CeO_2 content of 70%, the appearance of Fig. 3 suggests that in the cubic samples the reduction process is favored by substitution of Ce^{4+} with Zr^{4+}, while in the tetragonal one, the channel radius remains almost constant despite the decreasing cell dimensions. This is due to the increasing tetragonality of the samples. This consideration shows that in the cubic structure, oxygen mobility should be favored by substitution of the smaller Zr^{4+} cation for the larger Ce^{4+}.

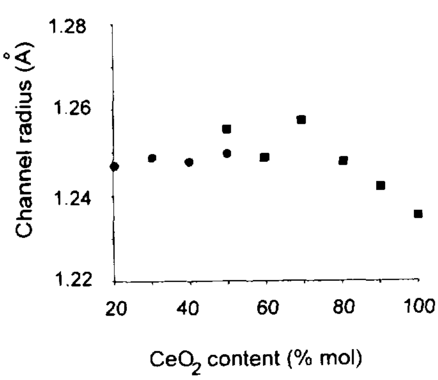

FIG. 3. Channel radius for oxygen hopping in the tetragonal (●) and cubic (■) structures.

There is, however, another intriguing observation which must not be forgotten in a rationalization of the TPR results. As shown in Table 1, apart from variation of lattice parameters, the incorporation of Zr^{4+} into the lattice strongly favors creation of structural defects. The importance of defective chemistry in catalysis (34) and particularly in the metal/CeO_2 systems is being widely recognized (2, 3). Most of the studies showed the crucial role of the metal/oxide interface in promoting oxygen exchange. Participation of lattice oxygen in the CeO_2 reduction/reoxidation phenomena was recognized by Jin *et al.* (35) in the temperature programmed desorption of CO and CO_2 from a Pt/CeO_2 catalyst. Subsequently, CO and CO_2 dissociation was found to be strongly enhanced after a high temperature reduction which was associated with creation of oxygen vacancies at the Rh/CeO_2 interface (14). Similarly, prereduced Pt/CeO_2 catalysts (36) showed a strong enhancement of CO oxidation activity, while for a model Rh/CeO_2 catalyst evidence for a second CO oxidation mechanism under reducing conditions was recently reported (37). Generally speaking, all these investigations point out the important role of surface oxygen vacancies or surface oxygen nests (38) in determining the catalytic behavior of M/CeO_2 systems. Recent evidence, however, shows that even long-range effects involving bulk CeO_2 lattice oxygen may play an important role in these phenomena. CO TPD from a Rh/CeO_2 catalyst showed that migration of lattice oxygen from CeO_2 to the metal occurs (25). Accordingly, the oxygen storage capacity was increased by formation of a La_2O_3–CeO_2 solid solution in Pt, Rh/La_2O_3–CeO_2/Al_2O_3 catalysts which was attributed to formation of lattice oxygen vacancies due to La^{3+} incorporation (39).

Structural defects are therefore expected to play an important role in determining the reduction/reoxidation behavior of the present samples. The cell volume decreases with increasing ZrO_2 content due to the smaller Zr^{4+} ionic diameter. It appears that in the cubic structure, the stress induced by the decrease of unit cell volume strongly favors formation of defects as is indicated in Table 1 by the decrease of the MO_2 unit. By contrast, in the tetragonal structure, the cell expansion along the c axis seems to compensate the stress induced by cell contraction, keeping the amount of structural defects almost constant. Even though quantitative estimation of the contribution of the defects to the oxygen mobility cannot be made, the overall suggestion is that their contribution will still enhance the oxygen mobility with increasing ZrO_2 amount in the cubic structure, while in the tetragonal structure this contribution should be constant. Therefore, on the basis of all the above considerations we prefer to attribute the shift toward higher temperatures observed in the TPR of the tetragonal samples to anisotropy of the oxygen mobility due to increasing tetragonality of these samples. Moreover, it should be noted that both $Ce_{0.3}Zr_{0.7}O_2$ and $Ce_{0.4}Zr_{0.6}O_2$ show presence of the three phases. Sample inhomogeneity due to the presence of different phases strongly decreased the ionic conductivity of calcia-stabilized zirconias (31c).

The presence of the LT and HT peaks shown in Fig. 1 and the increase of the LT/HT ratio with increasing ZrO_2 content (Table 2) can be attributed to a defect clustering induced by the reduction process (23a, 23c). At low degrees of reduction, only few randomly distributed Ce^{3+} sites are present in the lattice. However, at higher degrees of reduction an increasing amount of positively and negatively charged defects is present which will tend to cluster, making the ionic transport more difficult. In the fluorite oxides, for defect concentration above 0.08, the activation energy for the mass transport increases with increasing defect concentrations (25a). Consistently, when a degree of reduction $1.92 < x < 1.87$ is reached, i.e., after the LT peak, the reduction process is slowed down and further reduction occurs only at higher temperatures, i.e., the HT peak. Oxygen self-diffusion coefficients of 2.30×10^{-8} and 1.02×10^{-8} cm² s⁻¹ at 1673 and 1573 K, respectively, were found for a tetragonal $Ce_{0.12}Zr_{0.84}O_2$ (27). From these values, at a temperature of 1000 K, a displacement of 0.2 μm min^{-1} can be estimated. This estimate appears to be reliable since a diffusion coefficient of 13×10^{-17} cm^2 s^{-1} is calculated at 673 K which is comparable to the value of 16×10^{-17} cm^2 s^{-1} reported for a Rh/CeO_2 catalyst by Martin and Duprez (40). Defective structure accelerates oxygen diffusion in the bulk (41). SEM micrographs of our samples showed an average particle diameter of 1–6 μm. This suggests that the reduction process might be slow enough to allow defect ordering to occur providing an extra stabilization energy which hinders the oxygen mobility, thus accounting for the HT feature. In agreement with this attribution, on decreasing the CeO_2 content, the intensity of the HT peak diminishes, since more and more Ce^{4+} is reduced before defect clustering can occur.

As far as the $Rh/Ce_{0.1}Zr_{0.9}O_2$ sample is concerned, the above consideration cannot account for the appearance of the broad peak centered at 925 K since no preferential channels for oxygen migration are present in the monoclinic phase.

The OSC values reported in Table 3 appear to be strictly related to reduction behavior of the present samples, as the highest OSC value and lowest activation energy is found for the cubic $Rh/Ce_{0.5}Zr_{0.5}O_2$ sample. As stated above, the oxygen uptake measured by the pulse method is controlled by the oxygen mobility (22). In these conditions, the activation energy can be obtained from a $\ln(NT)$ vs. $1/T$ plot according to the relation (22)

$$NT \propto \mu_0 \exp(E/RT),$$

where N is the amount of O_2 uptake.

The activation energy of 3.4 kcal mol^{-1} observed for the Rh/CeO_2 sample is consistent with the value of 3.6 kcal mol^{-1} calculated from the cumulative OSC reported by Yao and Yao (1d), while it is about half of that reported by Cho (22). The decrease of the activation energy for oxygen uptake in the CeO_2–ZrO_2 samples appears to be correlated with decreasing LT peak temperatures of the three samples examined. As stated above, the defective structure accelerates oxygen diffusion in the bulk and accordingly the lowest activation energy for oxygen uptake is found in the cubic $Rh/Ce_{0.5}Zr_{0.5}O_2$ sample. Moreover, formation of Ce^{3+} upon reduction gives an expansion to the lattice of the CeO_2–ZrO_2 solid solution (9c). This more open structure could favor the reverse reoxidation accounting for the lower activation energy.

It was found (42) that upon O_2 adsorption over a partially reduced CeO_2, formation of surface peroxide species is strongly favored which was associated with a large number of surface defect sites formed by the reduction. Peroxide species can be considered as an intermediate which are formed in the dissociation of dioxygen over CeO_{2-x} surface to give the lattice oxygen ion O^{2-}. Therefore the overall OSC capacity is strongly related to the presence of defective sites. As a matter of fact, the OSC of pure CeO_2 is enhanced by increase of surface area. Higher surface areas indeed favor reduction of CeO_2 and hence formation of surface defective sites. By contrast, insertion of zirconia into the CeO_2 lattice induces formation of defective sites also in the bulk. Consequently, the oxygen mobility in the bulk is strongly enhanced thus allowing all of the matter to participate to the redox processes and accounting for the high OSC observed in the present samples. This final observation confirms the fundamental role of the defective chemistry in determining the catalytic properties of the CeO_2-based catalyst.

ACKNOWLEDGMENTS

Professor Renzo Rosei, University of Trieste, is gratefully acknowledged for helpful discussions. We thank Dr. Roberta Sessoli, Dipartimento di Chimica, Università di Firenze (Florence) for the magnetic susceptibility measurements. The Ministero dell'Università e della Ricerca Scientifica (Roma) and the C.N.R. under "Progetto Finalizzato Chimica Fine II" are acknowledged for financial support.

REFERENCES

1. (a) Summers, J. C., and Ausen, S. A., *J. Catal.* **58,** 131 (1979); (b) Kim, G., *Ind. Eng. Chem. Prod. Res. Dev.* **21,** 267 (1982); (c) Taylor, K. C. *in* "Catalysis-Science and Technology" (J. R. Ander-

son, and M. Boudart, Eds.), Vol. 5 Springer-Verlag, Berlin, 1984; (d) Yao, H. C., and Yu Yao, Y. F., *J. Catal.* **86,** 254 (1984).
2. Nunan, J. G., Robota, H. J., Cohn, M. J., and Bradley, S. A., *J. Catal.* **133,** 309 (1992).
3. Harrison, B., Diwell, A. F., and Hallett, C., *Platinum Met. Rev.* **32,** 73 (1988); Diwell, A. F., Rajaram, R. R., Shaw, H. A., and Truex, T. J., *in* "Catalysis and Automotive Pollution Control II" (A. Crucq, Ed.), Studies in Surface Science and Catalysis, Vol. 71, pp. 139–152. Elsevier, Amsterdam, 1991; Munuera, G., Fernandez, A. and Gonzalez-Elipe, A. R., *in* "Catalysis and Automotive Pollution Control II" (A. Crucq, Ed.), Studies in Surface Science and Catalysis, Vol. 71, pp. 207–219. Elsevier, Amsterdam, 1991.
4. Ranga Rao, G., Kašpar, J., Meriani, S., di Monte, R., and Graziani, M., *Catal. Lett.* **24,** 107 (1994).
5. Murota, T., Hagesawa, T., Aozasa, S., Matsui, H., and Motoyama, M., *J. Alloys Compounds* **193,** 298 (1993); Meriani, S., and di Monte, R., unpublished results.
6. McHale, A. E., "Phase Diagrams for Ceramists," Annual 1991, p. 20, Am. Ceram. Soc., Columbus, Ohio.
7. Pal'guev, S. F., Alyamosvkii, S. I., and Volchenkova, Z. S., *Russ. J. Inorg. Chem.* **4,** 1185 (1959).
8. Ranga Rao, G., Fornasiero, P., Kašpar, J., Meriani, S., di Monte, R., and Graziani, M., presented at "Catalysis and Automotive Pollution Control III," Bruxelles 1994, *Stud. Surf. Sci. Catal.*, submitted 1994; Kašpar, J. *et al.* to be submitted.
9. (a) Meriani, S., *Mater. Sci. Eng.* **71,** 369 (1985); (b) Meriani, S., and Spinolo, G., *Powder Diffraction* **2,** 255 (1987); (c) Meriani, S., *Mater. Sci. Eng. A* **109,** 121 (1989).
10. Yashima, M., Morimoto, K., Ishizawa, N., and Yoshimura, M., *J. Am. Ceram. Soc.* **76,** 1745 (1993).
11. Shannon, R. D., *Acta Crystallogr. Sect. A* **32,** 751 (1976).
12. Nuffield, E. W., "X-Ray Diffraction Methods." Wiley, New York, 1966.
13. Vis, J. C., van't Blik, H. F. J., Huizinga, T., van Grondelle, J., and Prins, R., *J. Catal.* **95,** 333 (1985).
14. Laachir, A., Perrichon, V., Badri, A., Lamotte, J., Catherine, E., Lavalley, J. C., El Fallah, J., Hilaire, L., le Normand, F., Quemere, E., Sauvion, N. S., and Touret, O., *J. Chem. Soc., Faraday Trans.* **87,** 1601 (1991).
15. Perrichon, V., Laachir, A., Beregeret, G., Fréty, R., and Tournayan, L., *J. Chem. Soc., Faraday Trans.* **90,** 773 (1994).
16. Trovarelli, A., Dolcetti, G., de Leitenburg, C., Kašpar, J., Finetti, P., and Santoni, A., *J. Chem. Soc. Faraday Trans.* **88,** 1311 (1992); Trovarelli, A., Dolcetti, G., de Leitenburg, C., and Kašpar, J., *in* "New Frontiers in Catalysis" (L. Guczi, F. Solymosi, and P. Tétényi, Eds.), Studies in Surface Science and Catalysis, Vol. 75, pp. 2781–2784.
17. Cunningham, J., Culliname, D., Sanz, J., Rojo, J. M., Soria, X. A., and Fierro, J. L. G., *J. Chem. Soc., Faraday Trans.* **88,** 3233 (1992).
18. Bernal, S., Calvino, J. J., Cifredo, G. A., Rodriguez-Izqueirdo, J. M., Perrichon, V., and Laachir, A., *J. Catal.* **137,** 1 (1992).
19. Ricken, M., Nolting, J., and Riess, I., *J. Solid State Chem.* **54,** 89 (1984).
20. Zotin, F. M. Z., Tournayan, L., Vardloud, J., Perrichon, V., and Fréty, R., *Appl. Catal. A: General* **98,** 99 (1993).
21. Fierro, J. L. G., Soria, J., Sanz, J., and Rojo, J. M., *J. Solid State Chem.* **66,** 154 (1987).
22. Cho, B. K., *J. Catal.* **131,** 74 (1991).
23. Bernal, S., Calvino, J. J., Cifredo, G. A., Rodriguez-Izquierdo, J. M., Perrichon, V., and Laachir, A., *J. Chem. Soc. Chem. Commun.*, 460 (1992).
24. Kubsch, J. E., Rieck, J. S., and Spencer, N. D., *in* "Catalysis and Automotive Pollution Control II", (A. Crucq, Ed.), Studies in Surface Science and Catalysis, Vol. 71, pp. 125–138, Elsevier, Amsterdam, 1991.
25. (a) Killner, J. A. and Steele, B. C. H., *in* "Non-Stoichiometric Oxides" (O.T. Sorensen, Ed.), Chap. 5, Academic Press, New York, 1981; (b) Matzke, H., *Ibidem* Chap. 4; (c) Catlow, C. R. A. *ibidem* Chap. 2.
26. Soria, J., Martinez-Arias, A. and Conesa, J. C., *Vacuum* **43,** 437 (1992).
27. Zafiris, G. S., and Gorte, J., *J. Catal.* **139,** 561 (1993).
28. Ando, K., Morita, S. and Watanabe, R., *Yogyo Kyokaishi* **94,** 732 (1986).
29. Crystal Data-Determinative Tables, Vol II, U.S. Department of Commerce, National Bureau of Standards, 1973.
30. Kofstad, P., "Nonstoichiometry, Diffusion, and Electrical Conductivity in Binary Oxides." Wiley, New York, 1972.
31. Fair, R. B., *J. Electrochem. Soc.* **122,** 800 (1975).
32. (a) Powers, R. W. and Mitoff, S. P. *in* "Solid Electrolytes General Principles, Characterization, Materials, Applications", Chap. 9, Academic Press, New York 1978; (b) Haven, Y., *ibidem*, Chap. 5; (c) R. M. and Hooper, A., *ibidem*, Chap. 18.
33. Etsell, T. H., and Flengas, S. N., *Chem. Rev.* **70,** 339 (1970).
34. Ilett, D. J. and Islam, M. S., *J. Chem. Soc., Faraday Trans.* **89,** 3833 (1993); for a recent review: Maire, J., *Angew. Chem.* **32,** 313, 528 (1993).
35. Jin, T., Okuhara, T., Mains, G. J., and White, J. M., *J. Phys. Chem.* **91,** 3310 (1987).
36. Serre, C., Garin, F., Belot, G., and Maire, G., *J. Catal.* **141,** 9 (1993).
37. Zafiris, G. S. and Gorte, J., *J. Catal.* **143,** 86 (1993).
38. Sanchez, M. G. and Gazquez, J. L., *J. Catal.* **104,** 120 (1987).
39. Miki, T., Ogawa, T., Haneda, M., Kakuta, N., Ueno, A., Tateishi, S., Matsuura, S., and Sato, M., *J. Phys. Chem.* **94,** 644 (1990).
40. Martin, D. and Duprez, D., *in* "New Aspects of Spillover Effects in Catalysis" (T. Inui, K. Fujimoto, T. Uchijima, and M. Masai, Eds.), Studies in Surface Science and Catalysis, Vol. 77, p. 201. Elsevier, Amsterdam, 1993.
41. Heussner, K. H., and Claussen, N., *J. Am. Ceram. Soc.* **72,** 1044 (1989).
42. Li, C., Domen, K., Maruya, K., and Onishi, T., *J. Am. Chem. Soc.* **111,** 7683 (1989).